A Three-Dimensional Finite-Difference Time-Domain Algorithm Based on the Recursive Convolution Approach For Propagation of Electromagnetic Waves in Nonlinear Dispersive Media

S. J. Yakura, J. T. MacGillivray and D. Dietz

Air Force Research Laboratory, Directed Energy Directorate
Kirtland AFB, NM 87117-5776

Abstract—We present for the first time a successful formulation of a three-dimensional finite-difference time-domain algorithm that is based on the recursive convolution approach and is used to evaluate the propagation of electromagnetic waves in nonlinear dispersive media. We treat in particular the case where the nonlinear polarization term depends only on the product of the square of the electric field and the third-order electric susceptibility function. However, the approach is general and we can easily extend the formulation to the product of any power of the electric field with the nth-order electric field susceptibility function. We find that, in contrast to the usual formulation for linear dispersive materials which uses a simple linear relationship between the next-time-step electric field and the previous-time-step electric field, the formulation for nonlinear dispersive materials with a third-order susceptibility function results in coupled nonlinear cubic equations which relate the next-time-step electric field vector to the previous-time-step electric field vector. Consequently, the coupled nonlinear cubic equations must be solved at each time step to advance the electric field vector.

I. INTRODUCTION

There has been considerable interest in understanding the transient behavior of an ultrafast laser pulse that interacts with a nonlinear dispersive material. In the last several years many experimentalists have made use of newly developed Kerr lens mode-locked titanium-sapphire lasers to perform well-controlled experiments to obtain accurate measurements of the transient behavior of ultrafast laser pulses in simple molecular liquids and solids which are known to exhibit nonlinear optical behavior [1]. To better understand the details of nonlinear processes that are observed in the experiments, numerical simulations have been used extensively to reproduce observed nonlinear effects. Until recently most computer simulation has been performed by solving an approximation to Maxwell's equations, known as the generalized nonlinear Schrödinger (GNLS) equation [2], to get information about the time evolution of the envelope of the propagating oscillating wave packet in order to obtain the overall shape of the propagating optical pulse. Because a GNLS equation-based computer simulation does not provide any information about the details of the oscillating waves inside the envelope of the optical pulse, there is a renewed interest in solving Maxwell's equations directly without having to rely on any approximations.

Happily, with the advent of present day computers which provide very fast execution times and great quantities of computer memory, we are at the point where enough computational power is available to solve Maxwell's equations directly for nonlinear dispersive materials. Among recently investigated numerical techniques that show great promise in achieving this goal is the well-known finite-difference time-domain (FDTD) method [3]. It is based on using a simple differencing scheme in both time and space to calculate the transient behavior of electromagnetic field quantities. Because of the usefulness of the FDTD method for many optical applications, recent researchers have focused their attention to the numerical evaluation of the linear and nonlinear polarization terms which appear in one of Maxwell's equations (Ampère's Law) as convolution integrals. An efficient evaluation of these terms allows us to model linear and nonlinear dispersive effects more effectively [4-9].

The designation of terms as linear and nonlinear depends upon the form of the integrand appearing in the convolution integral that relates the displacement field vector, $\underline{D}(t;\underline{x})$, to the electric field vector, $\underline{E}(t;\underline{x})$. For linear dispersive, isotropic materials, the relationship between $\underline{D}(t;\underline{x})$ and $\underline{E}(t;\underline{x})$ is usually expressed as

$$\underline{D}(t;\underline{x}) = \epsilon_o \epsilon_\infty \underline{E}(t;\underline{x}) + \epsilon_o \sum_{\rho=1}^{\rho_{max}} \int_{-\infty}^{\infty} \underline{E}(\tau;\underline{x}) X_\rho^{(1)}(t-\tau)\, d\tau \tag{1.1}$$

where ϵ_o is the electric permittivity of free space, ϵ_∞ is the medium permittivity at infinite frequency, and $X_\rho^{(1)}(t-\tau)$ is the ρth term of the collection consisting of ρ_{max} time dependent, first-order electric susceptibility functions, where ρ_{max} is the maximum number of terms which we choose to consider for a particular formulation of Eq. (1.1). For isotropic materials that exhibit both linear and nonlinear polarization properties, specifically through the first-order (linear) and third-order (nonlinear) electric susceptibility functions, $X_\rho^{(1)}(t-\tau)$ and $X_\rho^{(3)}(t,\tau,t_1,t_2)$, respectively, the

relationship between $\underline{D}(t;\underline{x})$ and $\underline{E}(t;\underline{x})$ can be expressed as [10]

$$\underline{D}(t;\underline{x}) = \epsilon_o \epsilon_\infty \underline{E}(t;\underline{x}) + \epsilon_o \sum_\rho \int_{-\infty}^{\infty} \underline{E}(\tau;\underline{x}) X_\rho^{(1)}(t-\tau)\, d\tau + \epsilon_o \sum_\rho \int_{-\infty}^{\infty}\int_{-\infty}^{\infty}\int_{-\infty}^{\infty} \underline{E}(t_2;\underline{x}) \left[\underline{E}(t_1;\underline{x}) \bullet \underline{E}(\tau;\underline{x})\right] \cdot X_\rho^{(3)}(t,\tau,t_1,t_2)\, dt_2\, dt_1\, d\tau \quad (1.2)$$

where $X_\rho^{(3)}(t,\tau,t_1,t_2)$ is the ρth term of the four-time dependent third-order susceptibility function which contributes to the nonlinear behavior of the material and $\bullet$ is the notation used for the dot product of vectors. When $X_\rho^{(3)}(t,\tau,t_1,t_2)$ is reduced to the single-time dependent susceptibility function, $\chi_\rho^{(3)}(t_1-t_2)$, by making use of the following Born-Oppenheimer approximation [10]

$$X_\rho^{(3)}(t,\tau,t_1,t_2) = \delta(\tau-t_1)\,\delta(t-t_2) \cdot \left[\chi_\rho^{(3)}(t_2-t_1) + \delta(t_2-t)\,\alpha_{0\rho}^{(3)}\right] \quad (1.3)$$

where $\alpha_{o\rho}^{(3)}$ is a constant and $\delta(t)$ is the Dirac delta function, we can show that Eq. (1.2) reduces to an expression that consists of sums of convolution integrals of linear and nonlinear terms; namely,

$$\underline{D}(t;\underline{x}) = \epsilon_o \epsilon_\infty \underline{E}(t;\underline{x}) + \epsilon_o \sum_\rho \int_{-\infty}^{\infty} \underline{E}(\tau;\underline{x}) X_\rho^{(1)}(t-\tau)\, d\tau + \epsilon_o\, \underline{E}(t;\underline{x}) \sum_\rho \int_{-\infty}^{\infty} \left[\underline{E}(\tau;\underline{x}) \bullet \underline{E}(\tau;\underline{x})\right] \chi_\rho^{(3)}(t-\tau)\, d\tau + \epsilon_o\, \underline{E}(t;\underline{x}) \left[\underline{E}(t;\underline{x}) \bullet \underline{E}(t;\underline{x})\right] \sum_\rho \alpha_{o\rho}^{(3)} \quad (1.4)$$

Based on the above expression, this paper provides a general formulation of the FDTD method, which we call the NonLinear Piecewise Linear Recursive Convolution (NLPLRC) approach, to evaluate the linear and nonlinear convolution integrals. We investigate in particular the case in which both the first-order and third-order electric susceptibility functions are expressed as complex functions that contain complex constant coefficients and exhibit exponential behavior in the time domain as follows:

$$\chi_\rho^{(1)}(t) = Re\left\{\alpha_\rho^L \exp(-\gamma_\rho^L t)\right\} U(t) \quad (1.5)$$

$$\chi_\rho^{(3)}(t) = Re\left\{\alpha_\rho^{NL} \exp(-\gamma_\rho^{NL} t)\right\} U(t) \quad (1.6)$$

where $Re\{\ \}$ is used to represent the real part of a complex function, $U(t)$ is the unit step function, and α_ρ^L, α_ρ^{NL}, γ_ρ^L and γ_ρ^{NL} are complex constant coefficients; superscripts L and NL are used to distinguish between linear and nonlinear coefficients. By making the proper choices of complex constant coefficients and performing Fourier transforms, we can readily obtain the familiar Debye and Lorentz forms of the complex permittivity in the frequency domain.

II. GOVERNING EQUATIONS AND GENERAL FORMULATION OF THE RECURSIVE CONVOLUTION APPROACH

In light of Eq. (1.4), Maxwell's equations inside the dispersive material can be written as

$$\nabla \times \underline{E}(t;\underline{x}) = -\frac{\partial[\mu \underline{H}(t;\underline{x})]}{\partial t} \quad (2.1)$$

$$\nabla \times \underline{H}(t;\underline{x}) = \frac{\partial \underline{D}(t;\underline{x})}{\partial t} + \sigma \underline{E}(t;\underline{x}) \quad (2.2)$$

with

$$\underline{D}(t;\underline{x}) = \epsilon_o \epsilon_\infty \underline{E}(t;\underline{x}) + \epsilon_o \sum_\rho \underline{P}_\rho^L(t;\underline{x}) + \epsilon_o\, \underline{E}(t;\underline{x}) \sum_\rho P_\rho^{NL}(t;\underline{x}) + \epsilon_o\, \underline{E}(t;\underline{x}) \left[\underline{E}(t;\underline{x}) \bullet \underline{E}(t;\underline{x})\right] \sum_\rho \alpha_{0\rho}^{(3)} \quad (2.3)$$

$$\underline{P}_\rho^L(t;\underline{x}) \equiv \int_{-\infty}^{\infty} \underline{E}(\tau;\underline{x})\, X_\rho^{(1)}(t-\tau)\, d\tau \quad (2.4)$$

$$P_\rho^{NL}(t;\underline{x}) \equiv \int_{-\infty}^{\infty} \left[\underline{E}(\tau;\underline{x}) \bullet \underline{E}(\tau;\underline{x})\right] \chi_\rho^{(3)}(t-\tau)\, d\tau \quad (2.5)$$

where $\underline{H}(t;\underline{x})$ is the magnetic field vector, μ is the magnetic permeability, and $\underline{P}_\rho^L(t;\underline{x})$ and $[\underline{E}(t;\underline{x})P_\rho^{NL}(t;\underline{x})]$ are related to the ρth terms of linear and nonlinear polarization field vectors, respectively. Using an FDTD algorithm, the above equations can be solved numerically at each time step provided we can handle $\underline{P}_\rho^L(t;\underline{x})$ and $P_\rho^{NL}(t;\underline{x})$ numerically. Therefore, the whole solution rests on the question of how to carry out the numerical evaluation of $\underline{P}_\rho^L(t;\underline{x})$ and $P_\rho^{NL}(t;\underline{x})$ at each successive time step. For that reason, the rest of this section is devoted to the numerical formulation that treats $\underline{P}_\rho^L(t;\underline{x})$ and $P_\rho^{NL}(t;\underline{x})$ based on the recursive convolution approach.

To obtain second-order accuracy in time in evaluating the convolution integrals, $\underline{E}(t;\underline{x})$ is taken to be a piecewise linear continuous function over the entire temporal integration range so that $\underline{E}(t;\underline{x})$ changes linearly with respect to time over a given discrete time interval $[m\Delta t,\ (m+1)\Delta t]$, where $m=0,1,\ldots,n$, with $n\Delta t$ being the current time step [11,12]. Referring to Figure 1, we can express $\underline{E}(t;\underline{x})$ in the following form in terms of the electric field values, $\underline{E}_{ijk}^{\,m}$ and $\underline{E}_{ijk}^{\,m+1}$, which are, respectively, evaluated at discrete time steps $t=m\Delta t$ and $t=(m+1)\Delta t$ and at the same discrete spatial location $\underline{x} = (i\Delta x, j\Delta y, k\Delta z)$ with Δx, Δy and Δz being the spatial grid sizes in the x, y and z directions, respectively (we use a superscript to designate the discrete time step and a subscript for the discrete spatial location):

$$\underline{E}(t;\underline{x}) = \begin{cases} \underline{E}_{ijk}^{m} + \dfrac{(\underline{E}_{ijk}^{m+1} - \underline{E}_{ijk}^{m})}{\Delta t}(t - m\Delta t), \text{ for} \\ \quad 0 \le m\Delta t \le t \le (m+1)\Delta t \le (n+1)\Delta t; \\ 0, \text{ for } \ t \le 0 \end{cases} \tag{2.6}$$

When Eq. (2.6) is substituted into Eq. (2.4), we obtain after some manipulation the following expression for discrete values of $\underline{P}_{\rho}^{\,L}(t;\underline{x})$ at discrete time step $n\Delta t$ and discrete spatial location $(i\Delta x, j\Delta y, k\Delta z)$ [see Appendix for details]:

$$\underline{P}_{\rho}^{L}(n\Delta t; i\Delta x, j\Delta y, k\Delta z) \equiv (\underline{P}_{\rho}^{L})_{ijk}^{n} \equiv Re\{(\underline{Q}_{\rho}^{L})_{ijk}^{n}\} \tag{2.7}$$

where the discrete complex values, $(\underline{Q}_{\rho}^{\,L})_{ijk}^{\,n}$, are defined as

$$(\underline{Q}_{\rho}^{L})_{ijk}^{n} \equiv \sum_{m=0}^{n-1} \{ \underline{E}_{ijk}^{m} (\psi_{\rho,0}^{L})^{n,m} + (\underline{E}_{ijk}^{m+1} - \underline{E}_{ijk}^{m})(\psi_{\rho,1}^{L})^{n,m} \} \tag{2.8}$$

with

$$(\psi_{\rho,0}^{L})^{n,m} \equiv \alpha_{\rho}^{L} \int_{(n-m-1)\Delta t}^{(n-m)\Delta t} exp(-\gamma_{\rho}^{L}\tau)\, d\tau \tag{2.9}$$

$$(\psi_{\rho,1}^{L})^{n,m} \equiv \frac{\alpha_{\rho}^{L}}{\Delta t} \int_{(n-m-1)\Delta t}^{(n-m)\Delta t} [(n-m)\Delta t - \tau] \cdot exp(-\gamma_{\rho}^{L}\tau)\, d\tau \tag{2.10}$$

Similarly, substituting Eq. (2.6) into Eq. (2.5), we obtain after some manipulation the following expression for discrete values of $P_{\rho}^{\,NL}(t;\underline{x})$ at discrete time step $n\Delta t$ and discrete spatial location $(i\Delta x, j\Delta y, k\Delta z)$ [again, see Appendix for details]:

$$P_{\rho}^{NL}(n\Delta t; i\Delta x, j\Delta y, k\Delta z) \equiv (P_{\rho}^{NL})_{ijk}^{n} \equiv Re\{(Q_{\rho}^{NL})_{ijk}^{n}\} \tag{2.11}$$

where the discrete complex values, $(Q_{\rho}^{\,NL})_{ijk}^{\,n}$, are defined as

$$(\underline{Q}_{\rho}^{NL})_{ijk}^{n} \equiv \sum_{m=0}^{n-1} \{ \underline{E}_{ijk}^{m} \bullet \underline{E}_{ijk}^{m} (\psi_{\rho,0}^{NL})^{n,m} + 2\underline{E}_{ijk}^{m} \bullet (\underline{E}_{ijk}^{m+1} - \underline{E}_{ijk}^{m})(\psi_{\rho,1}^{NL})^{n,m} + (\underline{E}_{ijk}^{m+1} - \underline{E}_{ijk}^{m}) \bullet (\underline{E}_{ijk}^{m+1} - \underline{E}_{ijk}^{m})(\psi_{\rho,2}^{NL})^{n,m} \} \tag{2.12}$$

with

$$(\psi_{\rho,0}^{NL})^{n,m} \equiv \alpha_{\rho}^{NL} \int_{(n-m-1)\Delta t}^{(n-m)\Delta t} exp(-\gamma_{\rho}^{NL}\tau)\, d\tau \tag{2.13}$$

$$(\psi_{\rho,1}^{NL})^{n,m} \equiv \frac{\alpha_{\rho}^{NL}}{\Delta t} \int_{(n-m-1)\Delta t}^{(n-m)\Delta t} [(n-m)\Delta t - \tau] \cdot exp(-\gamma_{\rho}^{NL}\tau)\, d\tau \tag{2.14}$$

$$(\psi_{\rho,2}^{NL})^{n,m} \equiv \frac{\alpha_{\rho}^{NL}}{(\Delta t)^2} \int_{(n-m-1)\Delta t}^{(n-m)\Delta t} [(n-m)\Delta t - \tau]^2 \cdot exp(-\gamma_{\rho}^{NL}\tau)\, d\tau \tag{2.15}$$

After some manipulation we can show that the ψ's defined in Eqs. (2.9), (2.10), (2.13), (2.14) and (2.15) satisfy the following recursive relationships relating the next time step, $(n+1)\Delta t$, to the current time step, $n\Delta t$:

$$(\psi_{\rho,0}^{L})^{n+1,m} = exp(-\gamma_{\rho}^{L}\Delta t)(\psi_{\rho,0}^{L})^{n,m} \tag{2.16}$$

$$(\psi_{\rho,1}^{L})^{n+1,m} = exp(-\gamma_{\rho}^{L}\Delta t)(\psi_{\rho,1}^{L})^{n,m} \tag{2.17}$$

$$(\psi_{\rho,0}^{NL})^{n+1,m} = exp(-\gamma_{\rho}^{NL}\Delta t)(\psi_{\rho,0}^{NL})^{n,m} \tag{2.18}$$

$$(\psi_{\rho,1}^{NL})^{n+1,m} = exp(-\gamma_{\rho}^{NL}\Delta t)(\psi_{\rho,1}^{NL})^{n,m} \tag{2.19}$$

$$(\psi_{\rho,2}^{NL})^{n+1,m} = exp(-\gamma_{\rho}^{NL}\Delta t)(\psi_{\rho,2}^{NL})^{n,m} \tag{2.20}$$

It is important to mention that we are able to obtain the above recursive relationships only because both the linear and nonlinear susceptibility functions are expressed in the exponential forms shown in Eqs. (1.5) and (1.6).

When Eqs. (2.16) through (2.20) are used in Eqs. (2.8) and (2.12), respectively, for the next discrete time step, we get the following expressions for $(\underline{P}_\rho^{\,L})_{ijk}^{n+1}$ and $(P_\rho^{NL})_{ijk}^{n+1}$ based on the recursive relationships obtained for $(\underline{Q}_\rho^{\,L})_{ijk}^{n+1}$ and $(Q_\rho^{NL})_{ijk}^{n+1}$ in terms of $\underline{E}_{ijk}^{n+1}$, $\underline{E}_{ijk}^{n}$, $(\underline{Q}_\rho^{\,L})_{ijk}^{n}$ and $(Q_\rho^{NL})_{ijk}^{n}$ via Eqs. (2.16)-(2.20):

$$
\begin{aligned}
&(\underline{P}_\rho^{\,L})_{ijk}^{n+1} \equiv Re\{(\underline{Q}_\rho^{\,L})_{ijk}^{n+1}\} \\
&= Re\{\exp(-\gamma_\rho^L \Delta t)(\underline{Q}_\rho^{\,L})_{ijk}^{n} + \underline{E}_{ijk}^{n}(\psi_{\rho,0}^{L})^{n+1,n} \\
&+ (\underline{E}_{ijk}^{n+1} - \underline{E}_{ijk}^{n})(\psi_{\rho,1}^{L})^{n+1,n}\} \\
&= Re\{\exp(-\gamma_\rho^L \Delta t)(\underline{Q}_\rho^{\,L})_{ijk}^{n} + \underline{E}_{ijk}^{n}(\psi_{\rho,0}^{L})^{1,0} \\
&+ (\underline{E}_{ijk}^{n+1} - \underline{E}_{ijk}^{n})(\psi_{\rho,1}^{L})^{1,0}\}
\end{aligned}
\tag{2.21}
$$

$$
\begin{aligned}
&(P_\rho^{NL})_{ijk}^{n+1} \equiv Re\{(Q_\rho^{NL})_{ijk}^{n+1}\} \\
&= Re\{\exp(-\gamma_\rho^{NL} \Delta t)(Q_\rho^{NL})_{ijk}^{n} + \underline{E}_{ijk}^{n} \bullet \underline{E}_{ijk}^{n}(\psi_{\rho,0}^{NL})^{n+1,n} \\
&+ 2\,\underline{E}_{ijk}^{n} \bullet (\underline{E}_{ijk}^{n+1} - \underline{E}_{ijk}^{n})(\psi_{\rho,1}^{NL})^{n+1,n} \\
&+ (\underline{E}_{ijk}^{n+1} - \underline{E}_{ijk}^{n}) \bullet (\underline{E}_{ijk}^{n+1} - \underline{E}_{ijk}^{n})(\psi_{\rho,2}^{NL})^{n+1,n}\} \\
&= Re\{\exp(-\gamma_\rho^{NL} \Delta t)(Q_\rho^{NL})_{ijk}^{n} + \underline{E}_{ijk}^{n} \bullet \underline{E}_{ijk}^{n}(\psi_{\rho,0}^{NL})^{1,0} \\
&+ 2\,\underline{E}_{ijk}^{n} \bullet (\underline{E}_{ijk}^{n+1} - \underline{E}_{ijk}^{n})(\psi_{\rho,1}^{NL})^{1,0} \\
&+ (\underline{E}_{ijk}^{n+1} - \underline{E}_{ijk}^{n}) \bullet (\underline{E}_{ijk}^{n+1} - \underline{E}_{ijk}^{n})(\psi_{\rho,2}^{NL})^{1,0}\}
\end{aligned}
\tag{2.22}
$$

In the above expressions, $(\psi_{\rho,0}^{L})^{1,0}$, $(\psi_{\rho,1}^{L})^{1,0}$, $(\psi_{\rho,0}^{NL})^{1,0}$, $(\psi_{\rho,1}^{NL})^{1,0}$ and $(\psi_{\rho,2}^{NL})^{1,0}$ can be evaluated explicitly from Eqs. (2.9), (2.10), (2.13), (2.14) and (2.15) in terms of known complex linear and nonlinear susceptibility coefficients α_ρ^{L}, α_ρ^{NL}, γ_ρ^{L}, γ_ρ^{NL} and Δt as follows:

$$
\begin{aligned}
&(\psi_{\rho,0}^{L})^{1,0} \equiv \alpha_\rho^{L} \int_0^{\Delta t} \exp(-\gamma_\rho^{L}\tau)\, d\tau \\
&= \frac{\alpha_\rho^{L}}{\gamma_\rho^{L}}[1 - \exp(-\gamma_\rho^{L}\Delta t)]
\end{aligned}
\tag{2.23}
$$

$$
\begin{aligned}
&(\psi_{\rho,1}^{L})^{1,0} \equiv \frac{\alpha_\rho^{L}}{\Delta t} \int_0^{\Delta t} (\Delta t - \tau)\exp(-\gamma_\rho^{L}\tau)\, d\tau \\
&= \frac{\alpha_\rho^{L}}{\gamma_\rho^{L}}\left\{1 - \frac{1}{\gamma_\rho^{L}\Delta t}[1 - \exp(-\gamma_\rho^{L}\Delta t)]\right\}
\end{aligned}
\tag{2.24}
$$

$$
\begin{aligned}
&(\psi_{\rho,0}^{NL})^{1,0} \equiv \alpha_\rho^{NL} \int_0^{\Delta t} \exp(-\gamma_\rho^{NL}\tau)\, d\tau \\
&= \frac{\alpha_\rho^{NL}}{\gamma_\rho^{NL}}[1 - \exp(-\gamma_\rho^{NL}\Delta t)]
\end{aligned}
\tag{2.25}
$$

$$
\begin{aligned}
&(\psi_{\rho,1}^{NL})^{1,0} \equiv \frac{\alpha_\rho^{NL}}{\Delta t} \int_0^{\Delta t} (\Delta t - \tau)\exp(-\gamma_\rho^{NL}\tau)\, d\tau \\
&= \frac{\alpha_\rho^{NL}}{\gamma_\rho^{NL}}\left\{1 - \frac{1}{\gamma_\rho^{NL}\Delta t}[1 - \exp(-\gamma_\rho^{NL}\Delta t)]\right\}
\end{aligned}
\tag{2.26}
$$

$$
\begin{aligned}
&(\psi_{\rho,2}^{NL})^{1,0} \equiv \frac{\alpha_\rho^{NL}}{(\Delta t)^2} \int_0^{\Delta t} (\Delta t - \tau)^2 \exp(-\gamma_\rho^{NL}\tau)\, d\tau \\
&= \frac{\alpha_\rho^{NL}}{\gamma_\rho^{NL}}\left\{1 - \frac{2}{\gamma_\rho^{NL}\Delta t}\left[1 - \frac{1}{\gamma_\rho^{NL}\Delta t}[1 - \exp(-\gamma_\rho^{NL}\Delta t)]\right]\right\}
\end{aligned}
\tag{2.27}
$$

To demonstrate how the above terms are used in the FDTD calculation, we consider a full three-dimensional case in Cartesian coordinates. We use the usual Yee algorithm [3] for Eqs. (2.1) and (2.2). The space discretization is done according to the usual staggered-grid with central differencing scheme so that we will not discuss it further here. The time discretization for Eqs. (2.1) and (2.2) become

$$
\mu \underline{H}_{ijk}^{n+1/2} - \mu \underline{H}_{ijk}^{n-1/2} = -\Delta t[\underline{\nabla} \times \underline{E}_{ijk}^{n}] \tag{2.28}
$$

$$
\underline{D}_{ijk}^{n+1} - \underline{D}_{ijk}^{n} = \Delta t[\underline{\nabla} \times \underline{H}_{ijk}^{n+1/2}] - \Delta t\, \sigma \underline{E}_{ijk}^{n} \tag{2.29}
$$

Based on expressions obtained in Eqs. (2.3), (2.21) and (2.22), the left-hand side of Eq. (2.29) can be expressed in terms of $\underline{E}_{ijk}^{n+1}$ and $\underline{E}_{ijk}^{n}$ as

$$
\begin{aligned}
&\underline{D}_{ijk}^{n+1} - \underline{D}_{ijk}^{n} = \epsilon_o \epsilon_\infty (\underline{E}_{ijk}^{n+1} - \underline{E}_{ijk}^{n}) \\
&+ \epsilon_o \sum_\rho Re\{[\exp(-\gamma_\rho^{L}\Delta t) - 1][(\underline{Q}_\rho^{\,L})_{ijk}^{n}] \\
&\quad + \underline{E}_{ijk}^{n}(\psi_{\rho,0}^{L})^{1,0} + (\underline{E}_{ijk}^{n+1} - \underline{E}_{ijk}^{n})(\psi_{\rho,1}^{L})^{1,0}\} \\
&+ \epsilon_o \sum_\rho Re\{[\underline{E}_{ijk}^{n+1}\exp(-\gamma_\rho^{NL}\Delta t) - \underline{E}_{ijk}^{n}](Q_\rho^{NL})_{ijk}^{n} \\
&\quad + \underline{E}_{ijk}^{n+1}[(\underline{E}_{ijk}^{n} \bullet \underline{E}_{ijk}^{n})](\psi_{\rho,0}^{NL})^{1,0} \\
&\quad + 2\,\underline{E}_{ijk}^{n+1}[\underline{E}_{ijk}^{n} \bullet (\underline{E}_{ijk}^{n+1} - \underline{E}_{ijk}^{n})](\psi_{\rho,1}^{NL})^{1,0} \\
&\quad + \underline{E}_{ijk}^{n+1}[(\underline{E}_{ijk}^{n+1} - \underline{E}_{ijk}^{n}) \bullet (\underline{E}_{ijk}^{n+1} - \underline{E}_{ijk}^{n})](\psi_{\rho,2}^{NL})^{1,0}\} \\
&+ \epsilon_o [\underline{E}_{ijk}^{n+1}[(\underline{E}_{ijk}^{n+1} \bullet \underline{E}_{ijk}^{n+1})] - \underline{E}_{ijk}^{n}[(\underline{E}_{ijk}^{n} \bullet \underline{E}_{ijk}^{n})]] \sum_\rho \alpha_{0\rho}^{(3)}
\end{aligned}
\tag{2.30}
$$

When Eq. (2.30) is substituted into Eq. (2.29), we obtain the following coupled cubic equations which we need to solve for $\underline{E}_{ijk}^{n+1}$ in terms of the known fields quantities, $(\underline{Q}_\rho^{L})_{ijk}^{n}$, $(\underline{Q}_\rho^{NL})_{ijk}^{n}$, $\underline{E}_{ijk}^{n}$ and $\underline{H}_{ijk}^{n+1/2}$, which are calculated at previous time steps $t=n\Delta t$ and $t=(n+1/2)\Delta t$:

$$\underline{a}_0 + a_1 \underline{E}_{ijk}^{n+1} + [\underline{a}_2 \bullet \underline{E}_{ijk}^{n+1}]\underline{E}_{ijk}^{n+1} + a_3 [\underline{E}_{ijk}^{n+1} \bullet \underline{E}_{ijk}^{n+1}]\underline{E}_{ijk}^{n+1} = 0 \tag{2.31}$$

where $\underline{a}_0$, a_1, $\underline{a}_2$, and a_3 are given by

$$\begin{aligned}
\underline{a}_0 &= -\Delta t[\,\underline{\nabla} \times \underline{H}_{ijk}^{n+1/2}] + \Delta t\,\sigma \underline{E}_{ijk}^{n} \\
&- \epsilon_o \epsilon_\infty \underline{E}_{ijk}^{n} + \epsilon_o \sum_\rho Re\{[\exp(-\gamma_\rho^L \Delta t) - 1](\underline{Q}_\rho^L)_{ijk}^{n}\} \\
&+ \epsilon_o \underline{E}_{ijk}^{n} \sum_\rho Re\{(\psi_{\rho,0}^L)^{1,0} - (\psi_{\rho,1}^L)^{1,0}\} \\
&- \epsilon_o \underline{E}_{ijk}^{n} \sum_\rho Re\{(Q_\rho^{NL})_{ijk}^{n}\} - \epsilon_o \underline{E}_{ijk}^{n} [\underline{E}_{ijk}^{n} \bullet \underline{E}_{ijk}^{n}] \sum_\rho \alpha_{0\rho}^{(3)}
\end{aligned} \tag{2.32}$$

$$\begin{aligned}
a_1 &= \epsilon_o \epsilon_\infty + \epsilon_o \sum_\rho Re\{(\psi_{\rho,1}^L)^{1,0}\} \\
&+ \epsilon_o \sum_\rho Re\{\exp(-\gamma_\rho^{NL} \Delta t)(Q_\rho^{NL})_{ijk}^{n}\} \\
&+ \epsilon_o [\underline{E}_{ijk}^{n} \bullet \underline{E}_{ijk}^{n}] \sum_\rho Re\{(\psi_{\rho,0}^{NL})^{1,0} - 2(\psi_{\rho,1}^{NL})^{1,0} + (\psi_{\rho,2}^{NL})^{1,0}\}
\end{aligned} \tag{2.33}$$

$$\underline{a}_2 = 2\epsilon_o \underline{E}_{ijk}^{n} \sum_\rho Re\{(\psi_{\rho,1}^{NL})^{1,0} - (\psi_{\rho,2}^{NL})^{1,0}\} \tag{2.34}$$

$$a_3 = \epsilon_o \sum_\rho Re\{(\psi_{\rho,2}^{NL})^{1,0}\} + \sum_\rho \alpha_{0\rho}^{(3)} \tag{2.35}$$

Eq. (2.31) can be solved for $\underline{E}_{ijk}^{n+1}$ by using any standard root-finding numerical technique. One possible technique is the iterative nonlinear Newton-Raphson method with $\underline{E}_{ijk}^{n}$ as the initial guess for the start of the iterative procedure [13].

Upon completing the calculation of $\underline{E}_{ijk}^{n+1}$, we proceed to update $(\underline{Q}_\rho^{L})_{ijk}^{n+1}$ and $(Q_\rho^{NL})_{ijk}^{n+1}$ by making use of Eqs. (2.21) and (2.22).

With above formulation, we only need to consider updating Eqs. (2.21), (2.22), (2.28) and (2.31), respectively, for $(\underline{Q}_\rho^{L})_{ijk}^{n+1}$, $(Q_\rho^{NL})_{ijk}^{n+1}$, $\underline{H}_{ijk}^{n+1/2}$, and $\underline{E}_{ijk}^{n+1}$ at each time step for carrying out a complete computer simulation of the electric field response in nonlinear dispersive materials. The flow chart of numerical steps, that are required to update electromagnetic field quantities, for the recursive convolution approach is shown in Figure 2.

For the purely linear dispersive case, $\underline{a}_2$ and a_3, as well as some terms appearing in $\underline{a}_0$ and a_1, turn out to be zero. In this case we can solve for $\underline{E}_{ijk}^{n+1}$ directly without having to rely on the numerical root finding technique as discussed more in detail in the published literature [14-19].

III. EQUIVALENCE OF THE RECURSIVE CONVOLUTION APPROACH TO THE AUXILIARY DIFFERENTIAL EQUATION APPROACH

An alternative technique for solving the nonlinear dispersive problem is the so-called auxiliary differential equation approach [4-7]. The auxiliary differential equation approach is in fact equivalent to the recursive convolution approach as we now show.

To begin, we first substitute Eq. (1.5) into Eq. (2.4) and Eq. (1.6) into Eq. (2.5) and then differentiate these integrals with respect to time to obtain the following first-order differential equations for complex functions $\underline{Q}_\rho^{L}(t;\underline{x})$ and $Q_\rho^{NL}(t;\underline{x})$:

$$\frac{\partial \underline{Q}_\rho^{L}(t;\underline{x})}{\partial t} + \gamma_\rho^L \underline{Q}_\rho^{L}(t;\underline{x}) = \alpha_\rho^L \underline{E}(t;\underline{x}) \tag{3.1}$$

$$\begin{aligned}
&\frac{\partial Q_\rho^{NL}(t;\underline{x})}{\partial t} + \gamma_\rho^{NL} Q_\rho^{NL}(t;\underline{x}) \\
&\qquad = \alpha_\rho^{NL}[\underline{E}(t;\underline{x}) \bullet \underline{E}(t;\underline{x})]
\end{aligned} \tag{3.2}$$

From the above equations, the linear and nonlinear polarization vectors, $\underline{P}_\rho^{L}(t;\underline{x})$ and $[\underline{E}(t;\underline{x})P_\rho^{NL}(t;\underline{x})]$, can be obtained simply by taking the real parts of $\underline{Q}_\rho^{L}(t;\underline{x})$ and $[\underline{E}(t;\underline{x})Q_\rho^{NL}(t;\underline{x})]$, respectively. Now, solving these two equations *exactly* by using integrating factors $\exp(\gamma_\rho^L t)$ and $\exp(\gamma_\rho^{NL} t)$, respectively, and then integrating between $n\Delta t$ and $n\Delta t+\Delta t$, we have

$$\begin{aligned}
\underline{Q}_\rho^{L}(n\Delta t+\Delta t;\underline{x}) &= \exp(-\gamma_\rho^L \Delta t)\underline{Q}_\rho^{L}(n\Delta t;\underline{x}) \\
&+ \alpha_\rho^L \exp(-\gamma_\rho^L \Delta t) \int_{n\Delta t}^{n\Delta t+\Delta t} \underline{E}(\tau;\underline{x}) \exp[-\gamma_\rho^L (n\Delta t - \tau)]d\tau
\end{aligned} \tag{3.3}$$

$$\begin{aligned}
Q_\rho^{NL}(n\Delta t+\Delta t;\underline{x}) &= \exp(-\gamma_\rho^{NL} \Delta t) Q_\rho^{NL}(n\Delta t;\underline{x}) \\
&+ \alpha_\rho^{NL} \exp(-\gamma_\rho^{NL} \Delta t) \int_{n\Delta t}^{n\Delta t+\Delta t} [\underline{E}(\tau;\underline{x}) \bullet \underline{E}(\tau;\underline{x})] \\
&\qquad \cdot \exp[-\gamma_\rho^{NL}(n\Delta t - \tau)]d\tau
\end{aligned} \tag{3.4}$$

If $\underline{E}(\tau;\underline{x})$ is assumed to vary linearly in time between $n\Delta t$ and $n\Delta t+\Delta t$, as in the piecewise linear approximation of Eq. (2.6), we can substitute Eq. (2.6) into the right hand side (i.e. the inhomogeneous part) of Eqs. (3.3) and (3.4), respectively, to obtain the following expressions for $(\underline{Q}_\rho^{L})^{n+1}$

and $(Q_\rho^{NL})^{n+1}$ at discrete time step $(n\Delta t+\Delta t)$ and discrete spatial location $(i\Delta x, j\Delta y, k\Delta z)$:

$$\underline{Q}_\rho^L(n\Delta t+\Delta t; i\Delta x, j\Delta y, k\Delta z) \equiv (\underline{Q}_\rho^L)_{ijk}^{n+1}$$
$$= exp(-\gamma_\rho^L \Delta t)(\underline{Q}_\rho^L)_{ijk}^n + \underline{E}_{ijk}^n(\psi_{\rho,0}^L)^{1,0}$$
$$+(\underline{E}_{ijk}^{n+1} - \underline{E}_{ijk}^n)(\psi_{\rho,1}^L)^{1,0} \tag{3.5}$$

$$Q_\rho^{NL}(n\Delta t+\Delta t; i\Delta x, j\Delta y, k\Delta z) \equiv (Q_\rho^{NL})_{ijk}^{n+1}$$
$$= exp(-\gamma_\rho^{NL} \Delta t)(Q_\rho^{NL})_{ijk}^n + [(\underline{E}_{ijk}^n \bullet \underline{E}_{ijk}^n)](\psi_{\rho,0}^{NL})^{1,0}$$
$$+2[\underline{E}_{ijk}^n \bullet (\underline{E}_{ijk}^{n+1} - \underline{E}_{ijk}^n)](\psi_{\rho,1}^{NL})^{1,0}$$
$$+[(\underline{E}_{ijk}^{n+1} - \underline{E}_{ijk}^n) \bullet (\underline{E}_{ijk}^{n+1} - \underline{E}_{ijk}^n)](\psi_{\rho,2}^{NL})^{1,0} \tag{3.6}$$

In the auxiliary differential equation approach, we first use Eq. (2.29) to calculate the updated displacement field vector, $\underline{D}_{ijk}^{n+1}$. Then the electric field vector, $\underline{E}_{ijk}^{n+1}$, is updated from the following constitutive relationship, which is obtained from Eq. (2.3) by evaluating it at $t=(n+1)\Delta t$:

$$\underline{D}_{ijk}^{n+1} = \epsilon_o\epsilon_\infty \underline{E}_{ijk}^{n+1} + \epsilon_o \sum_\rho Re\{(\underline{Q}_\rho^L)_{ijk}^{n+1}\}$$
$$+\epsilon_o \underline{E}_{ijk}^{n+1} \sum_\rho Re\{(Q_\rho^{NL})_{ijk}^{n+1}\}$$
$$+\epsilon_o \underline{E}_{ijk}^{n+1}[\underline{E}_{ijk}^{n+1} \bullet \underline{E}_{ijk}^{n+1}] \sum_\rho \alpha_{0\rho}^{(3)} \tag{3.7}$$

When Eqs. (3.5) and (3.6) are substituted into the above equation, we obtain the following coupled cubic equations which we need to solve for $\underline{E}_{ijk}^{n+1}$ in terms of the known field quantities, $\underline{D}_{ijk}^{n+1}$, $(\underline{Q}_\rho^L)_{ijk}^n$, $(Q_\rho^{NL})_{ijk}^n$, $\underline{E}_{ijk}^n$ and $\underline{H}_{ijk}^{n+1/2}$:

$$\underline{b}_0 + b_1 \underline{E}_{ijk}^{n+1} + [\underline{b}_2 \bullet \underline{E}_{ijk}^{n+1}] \underline{E}_{ijk}^{n+1}$$
$$+b_3 [\underline{E}_{ijk}^{n+1} \bullet \underline{E}_{ijk}^{n+1}] \underline{E}_{ijk}^{n+1} = 0 \tag{3.8}$$

where $\underline{b}_0$, b_1, $\underline{b}_2$, and b_3 are given by

$$\underline{b}_0 = -\underline{D}_{ijk}^{n+1} + \epsilon_o \sum_\rho Re\{exp(-\gamma_\rho^L \Delta t)(\underline{Q}_\rho^L)_{ijk}^n\}$$
$$+\epsilon_o \underline{E}_{ijk}^n \sum_\rho Re\{(\psi_{\rho,0}^L)^{1,0} - (\psi_{\rho,1}^L)^{1,0}\} \tag{3.9}$$

$$b_1 = \epsilon_o\epsilon_\infty + \epsilon_o \sum_\rho Re\{(\psi_{\rho,1}^L)^{1,0}\}$$
$$+\epsilon_o \sum_\rho Re\{exp(-\gamma_\rho^{NL} \Delta t)(Q_\rho^{NL})_{ijk}^n\}$$
$$+\epsilon_o [\underline{E}_{ijk}^n \bullet \underline{E}_{ijk}^n] \sum_\rho Re\{(\psi_{\rho,0}^{NL})^{1,0} - 2(\psi_{\rho,1}^{NL})^{1,0} + (\psi_{\rho,2}^{NL})^{1,0}\} \tag{3.10}$$

$$\underline{b}_2 = 2\epsilon_o \underline{E}_{ijk}^n \sum_\rho Re\{(\psi_{\rho,1}^{NL})^{1,0} - (\psi_{\rho,2}^{NL})^{1,0}\} \tag{3.11}$$

$$b_3 = \epsilon_o \sum_\rho Re\{(\psi_{\rho,2}^{NL})^{1,0}\} + \sum_\rho \alpha_{0\rho}^{(3)} \tag{3.12}$$

But we know that $\underline{D}_{ijk}^{n+1}$, which are found in the right hand side of Eq. (3.9), can be expressed as follows from Eq. (2.29):

$$\underline{D}_{ijk}^{n+1} = \underline{D}_{ijk}^n + \Delta t[\nabla \times \underline{H}_{ijk}^{n+1/2}] - \Delta t\, \sigma \underline{E}_{ijk}^n \tag{3.13}$$

Also, we can show from Eq. (2.3) that $\underline{D}_{ijk}^n$, which appear in the right hand side of the above equation, have the following forms when evaluated at $t=n\Delta t$:

$$\underline{D}_{ijk}^n = \epsilon_o\epsilon_\infty \underline{E}_{ijk}^n + \epsilon_o \sum_\rho Re\{(\underline{Q}_\rho^L)_{ijk}^n\}$$
$$+\epsilon_o \underline{E}_{ijk}^n \sum_\rho Re\{(Q_\rho^{NL})_{ijk}^n\}$$
$$+\epsilon_o \underline{E}_{ijk}^n [\underline{E}_{ijk}^n \bullet \underline{E}_{ijk}^n] \sum_\rho \alpha_{0\rho}^{(3)} \tag{3.14}$$

Now, substituting Eqs. (3.13) and (3.14) into Eq. (3.9), we can show that $\underline{b}_0$ is the same as $\underline{a}_0$ [see Eqs. (3.9) and (2.32)]; likewise, we can see that $b_1=a_1$ [see Eqs. (3.10) and (2.33)], $\underline{b}_2=\underline{a}_2$ [see Eqs. (3.11) and (2.34)], and $b_3=a_3$ [see Eqs. (3.12) and (2.35)]. Hence, we can conclude that the auxiliary differential equation approach is equivalent to the recursive convolution approach. The only difference is that the auxiliary differential equation approach requires additional memory to be allocated for the calculation of the displacement field vector, $\underline{D}(t;\underline{x})$, which is updated via Eq. (2.29) [or Eq. (3.13)] at each time step. Thus, in the auxiliary differential equation approach, we use Eqs. (2.28), (2.29), (3.5), (3.6) and (3.8) to update, respectively, for $\underline{H}_{ijk}^{n+1/2}$, $\underline{D}_{ijk}^{n+1}$, $(\underline{Q}_\rho^L)_{ijk}^{n+1}$, $(Q_\rho^{NL})_{ijk}^{n+1}$ and $\underline{E}_{ijk}^{n+1}$ at each time step in order to perform a complete simulation of the electric field response in nonlinear dispersive materials. Also shown in Figure 2 is the flow chart of numerical steps, required to update electromagnetic field quantities, for the auxiliary differential equation approach.

IV. NUMERICAL DEMONSTRATION: ONE- AND THREE-DIMENSIONAL CASE STUDIES FOR NONLINEAR SOLITARY WAVE FORMATION

A. One-dimensional Case

To demonstrate the validity of the NLPLRC algorithm, we first consider the formation of a temporal soliton in one-dimensional space inside a nonlinear dispersive medium. We simulate an optical pulse propagating into an infinite half-space nonlinear dispersive medium. First, we launch an optical pulse in free-space and propagate it from left to right

in the positive x-direction. After traveling a short distance, the optical pulse is incident on an infinite half-space nonlinear dispersive medium that is characterized by the first-order (linear) susceptibility function, $X_p^{(1)}(t)$, and the third-order (nonlinear) susceptibility function, $\chi_p^{(3)}(t)$. We consider the case where $X_p^{(1)}(t)$ and $\chi_p^{(3)}(t)$ are expressed in the following Lorentz forms [4,5] for a single species [i.e. set $\rho_{max} = 1$]:

$$X^{(1)}_{\rho=1}(t) = \frac{\omega_0^2(\epsilon_s - \epsilon_\infty)}{\sqrt{\omega_0^2 - \delta^2}} exp(-\delta t) \cdot sin(\sqrt{\omega_0^2 - \delta^2}\, t) \quad (4.1)$$

$$\chi^{(3)}_{\rho=1}(t) = \chi_{01}^{(3)}[(\tau_1^2 + \tau_2^2)/\tau_1 \tau_2^2] \cdot exp(-t/\tau_2) sin(t/\tau_1) \quad (4.2)$$

where ω_0 is the resonant frequency, ϵ_s is relative permittivity at DC, δ is the first-order susceptibility damping constant, $\chi_{01}^{(3)}$ is the Raman scattering nonlinear strength, $1/\tau_1$ is the optical phonon frequency, and τ_2 is the optical phonon lifetime.

Comparing Eqs. (4.1) and (4.2) with Eqs. (1.5) and (1.6), respectively, we can relate the above coefficients to the complex coefficients, which are introduced in Eqs. (1.5) and (1.6), as follows:

$$\alpha^L_{\rho=1} \Leftarrow i\frac{\omega_0^2(\epsilon_s - \epsilon_\infty)}{\sqrt{\omega_0^2 - \delta^2}} \quad (4.3)$$

$$\gamma^L_{\rho=1} \Leftarrow (\delta + i\sqrt{\omega_0^2 - \delta^2}) \quad (4.4)$$

$$\alpha^{NL}_{\rho=1} \Leftarrow i\chi_{00}^{(3)}[(\tau_1^2 + \tau_2^2)/\tau_1 \tau_2^2] \quad (4.5)$$

$$\gamma^{NL}_{\rho=1} \Leftarrow (\frac{1}{\tau_2} + i\frac{1}{\tau_1}) \quad (4.6)$$

where i is the imaginary unit.

We consider the incident optical pulse to have a sinusoidal-carrier electric field frequency, ω_c, of 8.61×10^{14} radians/sec which is enveloped inside a hyperbolic secant (sech) function that has a width constant, T_w, of 3.50 femtoseconds. The following mathematical form describes the time-dependent incident optical pulse that we use in our one-dimensional FDTD simulation:

$$Incident\ Optical\ Pulse(t) = A\ cos[\omega_c(t - t_{delay})] \cdot sech\left[\frac{(t - t_{delay})}{T_w}\right] \quad (4.7)$$

where A is the amplitude of the electric field and t_{delay} is the delay time for the incident optical pulse to reach its peak value. We arbitrarily assign A to take the value of 1.0 volt/meter and t_{delay} to take the value of 41.70 femtoseconds.

We select the total number of simulation cells to be 200,000, ranging from x = -10,000 to x = 190,000, with the free-space/dispersive-material interface located at x = 0. We launch an optical pulse into free space at the leftmost edge (at x = -10,000) and the optical pulse travels in the positive x-direction. We use the LIAO absorbing boundary condition [20] at both ends of the computational space. We placed enough buffer cells between the main part of the simulation volume and the outer boundary to minimize the effects of the outer absorbing boundary inside the main nonlinear interaction region.

Following are the basic FDTD parameters that we use in our one-dimensional simulation:

Uniform cell size (Δx) = 5 nanometers,
Total simulation distance = 0.1 centimeter
(i.e. Δx times the total number of cells),
Time step increment ($\Delta t = \Delta x/2c$)
= 0.00834 femtosecond,
Total number of time steps = 400,000
(or total simulation time = 3336 femtoseconds),
where c is the speed of light.

For Δx of 5 nanometers, we estimate the free space numerical phase velocity error to be around 5×10^{-6} [21], which is about the same order of accuracy as the single precision calculation of our SPARC UNIX workstations.

To compare our FDTD results with the results published by Goorjian and Taflove in their papers [4,5], we use values similar to theirs to describe the property of linear and nonlinear dispersive materials. Shown below are the values of linear and nonlinear dispersive material properties that we use in our one-dimensional FDTD simulation.

Linear dispersive material properties:

$\epsilon_s = 5.25$,
$\epsilon_\infty = 2.25$,
$\omega_0 = 8.0 \times 10^{14}$ radians/sec, and
$\delta = 4.0 \times 10^9$ (sec)$^{-1}$.

Nonlinear dispersive material properties:

$\tau_1 = 12.2$ femtoseconds and
$\tau_2 = 32.0$ femtoseconds.

To see the difference in linear and nonlinear responses, we first calculate the strictly linear dispersive case by setting both the Raman scattering nonlinear strength, $\chi_{01}^{(3)}$, and the Kerr-type instantaneous nonlinear coefficient, $\alpha_{01}^{(3)}$, to zero. For the nonlinear calculations, we investigate two extreme cases: the purely Kerr-type instantaneous nonlinear dispersive case with $\chi_{01}^{(3)} = 0$ and $\alpha_{01}^{(3)} = 0.2$ (volts/meter)$^{-2}$, and the purely Raman scattering (delayed) nonlinear dispersive case with $\chi_{01}^{(3)} = 2.0$ (volts/meter)$^{-2}$ and $\alpha_{01}^{(3)} = 0$.

To update the electric field value for the next time step, we use the simple Newton-Raphson iterative method by making use of the current-time-step electric field value as the initial

guess to solve the cubic equation [see Eq. (2.31)]. For all calculations we perform, the convergence criterion of 10^{-4} is satisfied with at most three iterations.

Shown in Figure 3, Figure 4 and Figure 5 are the spatial electric field patterns that we obtain for the strictly linear dispersive, the purely Kerr-type instantaneous nonlinear dispersive, and the purely Raman scattering nonlinear dispersive cases, respectively, at time steps of 20,000, 40,000, 200,000 and 350,000.

Figure 3 shows the usual optical pulse broadening due to the linear dispersive effect as the optical pulse propagates into the dispersive medium.

In Figure 4, we can see the beginning of the formation of a solitary wave packet for the purely Kerr-type instantaneous nonlinear dispersive case soon after the wave propagates into the nonlinear dispersive medium. First, it appears as the small spike-like shape inside the linearly dispersive part of the pulse as a result of the nonlinear self-focusing effect. As the pulse propagates deeper into the dispersive medium, the spike-like shape transforms gradually to the shape that resembles more of the solitary wave packet and becomes isolated from the main part of the linear dispersive pulse due to the slower speed of the moving solitary wave packet. Once the solitary wave packet becomes completely isolated from the linear dispersive part of the pulse, the solitary wave packet propagates at constant amplitude while maintaining the shape of the hyperbolic secant function for the wave packet (i.e. a solution of the nonlinear Schrödinger equation that describes the shape of the propagating solitary wave packet). Another feature seen in Figure 4 is the formation of a small secondary high frequency precursory wave packet that moves ahead of the linear dispersive part of the pulse and the nonlinear solitary wave packet. Others have also previously reported the appearance of the same secondary high frequency precursory pulse packet [4,22]. When we perform a frequency analysis of both the solitary wave packet and the secondary high frequency precursory wave packet, we find that the main peak of the secondary high frequency precursory wave packet lies exactly at three times that of the solitary wave packet [see Figure 6]. This is consistent with analysis done by Hile [22].

For the purely Raman scattering nonlinear dispersive case, we can see in Figure 5 the formation of a solitary wave packet that is similar to the one we obtain for the purely Kerr-type instantaneous nonlinear dispersive case; however, the solitary wave packet appears retarded in time behind the linear dispersive pulse due to the delayed nonlinear response. We also observe the appearance of the secondary high frequency wave packet, but at least four orders of magnitude smaller than that of the purely Kerr-type instantaneous nonlinear dispersive case.

When we compare the results of our FDTD approach with that of the auxiliary differential (ADE) approach reported by Goorjian and Taflove [4], we find that there is a significant difference in the purely Raman scattering nonlinear dispersive case. To get the results from Goorjian and Taflove's ADE approach, we coded their ADE algorithm as found in their paper and performed the FDTD calculation using exactly the same FDTD parameters as we have used in our FDTD calculation. The result is that for no value of $\chi_{01}^{(3)}$ could we produce the delayed solitary wave packet that resembles the shape we obtain in our FDTD calculation. However, when we compare the results for the strictly linear dispersive and purely Kerr-type instantaneous nonlinear dispersive cases, we obtain very good agreement. Figures 7, Figure 8 and Figure 9, respectively, show the comparisons of spatial electric field profiles between Goorjian and Taflove's ADE approach and our FDTD approach at a time step of 350,000 for the three cases which we have studied: 1. the strictly linear dispersive case; 2. the purely Kerr-type instantaneous nonlinear dispersive case; and 3. the purely Raman scattering nonlinear dispersive case. We believe that the different spatial electric field profiles obtained for the purely Raman scattering nonlinear dispersive case (see Figure 9) between our NLPLRC approach and Goorjian and Taflove's ADE approach is the result of an approximation used by Goorjian and Taflove in their ADE algorithm to update linear and nonlinear polarization values. In their ADE algorithm, they simply used the square of the current-time-step electric field value in place of the square of the time-dependent electric field function that appears in their linear and nonlinear polarization differential equations [Eqs. (15) and (16) in Ref. 4] to calculate the next-time-step linear and nonlinear polarization field values. Rather, we believe that they should have evaluated the time-dependent electric field as a function of both the current-time-step and the next-time-step electric field values to correctly update linear and nonlinear polarization values. By choosing only the current-time-step electric field value, they basically reduced their ADE algorithm to first-order accuracy for solving a set of nonlinear differential equations. If they had chosen to use both the current and next-time-step electric field values, they were faced with solving a complicated set of coupled nonlinear algebraic equations [Eqs. (15), (16) and (17) in Ref. 4] to update the next-time-step linear polarization field value, the next-time-step nonlinear polarization field value, and the next-time-step electric field value, in which they have avoided in favor of computational simplicity.

To assure ourselves of the computational correctness of the results that we obtained from NLPLRC algorithm, we repeated the same FDTD calculations using one-half the cell size and one-half the time step increment. These higher spatial and temporal resolution calculations resulted in a relative difference of less than 10^{-5} for the electric field value at the end of the simulation run. Since this relative difference is on the order of the single precision calculation error, we concluded that we are indeed calculating the correct electric field value. This procedure also served to validate the use of the piecewise linear approximation.

To make a physical interpretation of the result we obtained for our Raman scattering nonlinear dispersive case, we realize that the decay term [i.e. γ_ρ^{NL}] of the third-order (nonlinear) susceptibility function contributes to a certain amount of the delay before the nonlinear effects actually start to play a role. The delay should be on the order of the inverse decay term. Until that time the Raman scattering nonlinear dispersive case should behave much like the strictly linear dispersive case. Shown in Figure 10 are the snap shots of spatial electric field profiles of the three cases taken at the same time step of 350,000 for a direct comparison. From these plots we see that the result of the Raman scattering nonlinear dispersive case reveals exactly of these characteristics which are associated with the delayed time response. At the front of the propagating pulse, the linear dispersive effect contributes significantly. Only after the pulse propagates a certain distance (which corresponds to the time delay of $1/\gamma_\rho^{NL}$) the nonlinear feedback becomes significant enough to create the soliton-like structure in the tail end of the propagating pulse.

As far as computational performance is concerned, less than 0.2 microsecond of the CPU time is required to update all four electromagnetic field values per time step per cell using an ULTRA 60 SPARC UNIX workstation to perform 1-D NLPLRC based on a convergence criterion of 10^{-4}. This is about eight times that of the CPU time needed to update electric and magnetic field values in free space. When compared to Goorjian and Taflove's ADE approach, our NLPLRC approach takes about 20% less amount of time to update field values.

B. Three-dimensional Case

To demonstrate our NLPLRC algorithm in three-dimension, we investigate the dispersive effect of a propagating optical TE_{10} mode inside a square waveguide. First, we excite an optical TE_{10} mode at the center of the leftmost x-y plane of a free-space square waveguide using an electric dipole source that is driven by a Gaussian pulse. The excited optical TE_{10} mode propagates in the positive z-direction inside the free-space square waveguide and is incident on the x-y plane of the free-space/dispersive-medium interface. Then the transmitted wave propagates deeper into the right half-infinite volume of the dispersive medium. The free-space /dispersive-medium interface is located at $z = 0$, with $z < 0$ for free-space and $z > 0$ for the dispersive medium.

To perform three-dimensional FDTD calculations, we consider the same Lorentz forms for the first-order (linear) susceptibility function, $X_\rho^{(1)}(t)$, and the third-order (nonlinear) susceptibility function, $\chi_\rho^{(3)}(t)$, and assign the same values for linear and nonlinear material properties as we have used in the one-dimensional case. The basic FDTD parameters that we use in our three-dimensional simulation are shown below:

Dimensions of the square waveguide:
x = 0.6 micrometers,
y = 0.6 micrometers, and
z = 37.5 micrometers,
Uniform cubic cell size = 0.0015 micrometer
(i.e. $\Delta x=\Delta y=\Delta z$),
Number of Δx cells in the x direction = 40,
Number of Δy cells in the y direction = 40,
Number of Δz cells in the z direction = 2,500
(ranging from z = -1,000 to z = 1,500),
Time step increment = 0.025 femtosecond
(i.e. $\Delta t = \Delta x/2c$),
Number of time steps = 8000
(or total simulation time = 200 femtoseconds).

To excite an optical TE_{10} mode, we use the following expression for the time dependent Gaussian pulse:

$$Gaussian\ Pulse(t) = A_g \exp\left[-\left(\left(t - t_{gdelay}\right)/\eta_g\right)^2\right] \quad (4.8)$$

where A_g is the driving pulse amplitude with an arbitrarily assigned value of 100.0 volts/meter, η_g is the width of the Gaussian spread with an arbitrarily assigned value of 3.0 femtoseconds, and t_{gdelay} is the delay time to attain the peak value with an arbitrarily assigned value of 10.0 femtoseconds. Shown in Figure 11 are time-dependent electric field plots of the Gaussian driving pulse which excites an optical TE_{10} mode and the resulting optical TE_{10} mode incident at the center of the x-y plane of the free-space/dispersive medium interface.

We use the LIAO absorbing boundary condition at the left and right outermost x-y planes (at z = -1,000 and z =1,500) to absorb outgoing waves.

As we did in the one-dimensional case studies, we first calculate the strictly linear dispersive case by setting both Raman scattering nonlinear strength, $\chi_{01}^{(3)}$, and Kerr-type instantaneous nonlinear coefficient, $\alpha_{01}^{(3)}$, to zero. Then, we perform nonlinear calculations by considering two extreme cases: the purely Kerr-type instantaneous nonlinear dispersive case with $\chi_{01}^{(3)} = 0$ and $\alpha_{01}^{(3)} = 20{,}000$ (volts/meter)$^{-2}$, and the purely Raman scattering (delayed) nonlinear dispersive case with $\chi_{01}^{(3)} = 200{,}000$ (volts/meter)$^{-2}$ and $\alpha_{01}^{(3)} = 0$.

To update electric field values for the next time step, we use the nonlinear Newton-Raphson iterative method by making use of the current-time-step electric field values as the initial guess to solve the coupled cubic equations [see Eq. (2.31)]. During FDTD calculations, it is not uncommon to see the iterative method requiring more than 10 iterations to converge to the next-time-step electric field value based on a convergence criterion of 10^{-4} whenever nonlinear self focusing becomes strong.

Figure 12 shows a comparison of wave energy density spatial profiles inside the dispersive medium that we obtain from the strictly linear dispersive, the purely Kerr-type

instantaneous nonlinear dispersive, and from the purely Raman scattering nonlinear dispersive cases. These plots are taken at a time step of 7,500, which is late enough to observe distinct differences in the three cases. Based on these energy density plots shown in Figure 12, we can say that the three-dimensional case studies result in the same qualitative behavior as we saw in one-dimensional case studies.

V. CONCLUSIONS

Based on the NonLinear Piecewise Linear Recursive Convolution (NLPLRC) approach presented in this paper, we can show that it is possible to predict the formation of nonlinear solitary waves by solving Maxwell's equations directly for the propagation of electromagnetic waves in nonlinear dispersive media that exhibit both instantaneous Kerr (i.e. $\alpha_{01}^{(3)} \neq 0$) and Raman scattering (i.e. $\chi_{01}^{(3)} \neq 0$) responses. The NLPLRC approach is shown to be equivalent to the auxiliary differential equation approach provided that the auxiliary differential equations are solved analytically using integrating factors and that the same piecewise linear approximation is used for $\underline{E}(t;\underline{x})$ to integrate inhomogeneous parts of the auxiliary differential equations. Because we use a piecewise linear approximation for the time-dependent part of the electric field vector, the NLPLRC approach results in second-order accuracy in time. The NLPLRC approach retains all the advantages of the usual first-order discrete recursive convolution approach, such as fast computational speed and efficient use of computer memory; however, the NLPLRC approach provides second-order accuracy in time.

We point out again that the exponential forms of the linear and nonlinear susceptibility functions are crucial in allowing us to implement the recursive feature in our algorithm. Also, our FDTD formulation for nonlinear dispersive materials results in having to solve coupled nonlinear (cubic) equations for the three components of the electric field vector at each time step as compared to just solving linear equations in the case of linear dispersive materials.

APPENDIX

For the linear part, when we substitute Eq. (2.6) into Eq. (2.4) and evaluate t at $n\Delta t$ for the argument of the susceptibility function, where n denotes the nth time step, we have

$$(\underline{Q}_{\rho}^{L})_{ijk}^{n} = \sum_{m=0}^{n-1} \int_{m\Delta t}^{(m+1)\Delta t} \Big\{ \underline{E}_{ijk}^{m} + [\underline{E}_{ijk}^{m+1} - \underline{E}_{ijk}^{m}] \cdot \frac{1}{\Delta t}[\tau - m\Delta t] \Big\} X_{\rho}^{(1)}(n\Delta t - \tau)\, d\tau$$

$$= \sum_{m=0}^{n-1} \Big\{ \underline{E}_{ijk}^{m} \int_{m\Delta t}^{(m+1)\Delta t} X_{\rho}^{(1)}(n\Delta t - \tau) d\tau + [\underline{E}_{ijk}^{m+1} - \underline{E}_{ijk}^{m}] \frac{1}{\Delta t} \int_{m\Delta t}^{(m+1)\Delta t} [\tau - m\Delta t] X_{\rho}^{(1)}(n\Delta t - \tau)\, d\tau \Big\} \quad \text{(A.1)}$$

Similarly for the nonlinear part, when we substitute Eq. (2.6) into Eq. (2.5) and evaluate t at $n\Delta t$ for the argument of the susceptibility function where n is the nth time step, we have

$$(\underline{Q}_{\rho}^{NL})_{ijk}^{n} = \sum_{m=0}^{n-1} \int_{m\Delta t}^{(m+1)\Delta t} \Big\{ \underline{E}_{ijk}^{m} \bullet \underline{E}_{ijk}^{m} + 2\underline{E}_{ijk}^{m} \bullet [\underline{E}_{ijk}^{m+1} - \underline{E}_{ijk}^{m}] \frac{1}{\Delta t}[\tau - m\Delta t] + [\underline{E}_{ijk}^{m+1} - \underline{E}_{ijk}^{m}] \bullet [\underline{E}_{ijk}^{m+1} - \underline{E}_{ijk}^{m}] \frac{1}{(\Delta t)^2}[\tau - m\Delta t]^2 \Big\} \chi_{\rho}^{(3)}(n\Delta t - \tau)\, d\tau$$

$$= \sum_{m=0}^{n-1} \Big\{ \underline{E}_{ijk}^{m} \bullet \underline{E}_{ijk}^{m} \int_{m\Delta t}^{(m+1)\Delta t} \chi_{\rho}^{(3)}(n\Delta t - \tau)\, d\tau + 2\underline{E}_{ijk}^{m} \bullet [\underline{E}_{ijk}^{m+1} - \underline{E}_{ijk}^{m}] \frac{1}{\Delta t} \int_{m\Delta t}^{(m+1)\Delta t} [\tau - m\Delta t] \chi_{\rho}^{(3)}(n\Delta t - \tau)\, d\tau + [\underline{E}_{ijk}^{m+1} - \underline{E}_{ijk}^{m}] \bullet [\underline{E}_{ijk}^{m+1} - \underline{E}_{ijk}^{m}] \frac{1}{(\Delta t)^2} \int_{m\Delta t}^{(m+1)\Delta t} [\tau - m\Delta t]^2 \chi_{\rho}^{(3)}(n\Delta t - \tau)\, d\tau \Big\} \quad \text{(A.2)}$$

Using the change of variable $\tau' = (n\Delta t - \tau)$, we can readily show the existence of the following relationship for the above integrals:

$$\int_{m\Delta t}^{(m+1)\Delta t} [\tau - m\Delta t]^k f(n\Delta t - \tau) d\tau = \int_{(n-m-1)\Delta t}^{(n-m)\Delta t} [(n-m)\Delta t - \tau']^k f(\tau')\, d\tau' \quad \text{(A.3)}$$

where k takes the values of 0, 1, and 2 and $f(t)$ represents the time-dependent first order susceptibility function, $X_{\rho}^{(1)}(t)$, or the time-dependent third order susceptibility function, $\chi_{\rho}^{(3)}(t)$.

Since τ' appearing in the right-hand side of Eq. (A.3) is the integration variable, we can simply replace it by τ. When Eq. (A.3) is substituted back into Eqs. (A.1) and (A.2), we can obtain the expressions shown in Eqs. (2.8) and (2.12).

REFERENCES

[1] T-H. Huang, C-C. Hsu, T-H. Wei, S. Chang, S-M Yen, C-P. Tsai, R-T. Liu, C-T. Kuo, W-S. Tse and C. Chia, "The Transient Optical Kerr Effect of Simple Liquids Studied with an Ultrashort Laser with Variable Pulsewidth," IEEE Jour. of Selected Topics in Quantum Electronics, vol. 2, pp. 756-775, 1996

[2] K. J. Blow and D. Wood, 'Theoretical Description of Transient Stimulated Raman Scattering in Optical Fibers," IEEE Jour. of Quantum Electronics, vol. 25, pp. 2665-2673, 1989

[3] K. S. Yee, "Numerical Solution of Initial Boundary Value Problems Involving Maxwell's Equations in Isotropic Media," IEEE Trans. Antenna Propagat., vol. AP-14, pp. 302-307, 1966

[4] P. M. Goorjian, A. Taflove, R. M. Joseph and S. C. Hagness, 'Computational Modeling of Femtosecond Optical Solitons from Maxwell's Equations," IEEE J. of Quantum Electronics, vol. 28, pp. 2416-2422, 1992

[5] P. M. Goorjian, A. Taflove, "Direct Time Integration of Maxwell's Equations in Nonlinear Dispersive Media for Propagation of Femtosecond Electromagnetic Solitons," Opt. Lett., vol. 17, pp. 180-182, 1992

[6] R. M. Joseph, P. M. Goorjian and A. Taflove, "Direct Time Integration of Maxwell's Equations in Two-dimensional Dielectric Waveguides for Propagation and Scattering of Femtosecond Electromagnetic Solitons," Opt. Lett., vol. 18, pp. 491-493, 1993

[7] R. M. Joseph and A. Taflove, "Spatial Soliton Deflection Mechanism Indicated by FD-TD Maxwell's Equations Modeling," IEEE Photonics Tech. Lett., vol. 6, pp. 1251-1254, 1994

[8] R. W. Ziolkowski and J. B. Judkins, "Applications of the Nonlinear Finite Difference Time Domain (NL-FDTD) Method to Pulse Propagation in Nonlinear Media: Self Focusing and Linear Interfaces," Opt. Lett., vol. 18, pp. 491-493, 1993

[9] R. W. Ziolkowski and J. B. Judkins, "Full-wave Vector Maxwell Modeling of the Self-focusing of Ultrashort Optical Pulses in a Nonlinear Kerr Medium Exhibiting a Finite Response Time," Jour. Opt. Soc. Am B., vol. 10, pp. 186-198, 1993

[10] R. W. Hellworth, "Third-order Optical Susceptibility of Liquids and Solids," Prog. Quantum Electronics, vol. 5, pp. 1-68, 1977

[11] D. F. Kelley and R. J. Luebbers, "Piecewise Linear Recursive Convolution for Dispersive Media Using FDTD," IEEE Trans. Antenna and Propagat., vol. 44, pp. 792-797, 1996

[12] S. J. Yakura and J. MacGillivray, "Finite-Difference Time-Domain Calculations Based on Recursive Convolution Approach for Propagation of Electromagnetic Waves in Nonlinear Dispersive Media," Air Force Research Laboratory Report (PL-TR-97-1170), Oct 30, 1997.

[13] W. H. Press, S. A, Teukolsky, W. T. Vetterling and B. P. Flannery, *Numerical Recipes in FORTRAN - The Art of Scientific Computing Second Edition,* Chapter 9:Root Finding and Nonlinear Sets of Equations, pp. 372-375, Cambridge University Press, 1992

[14] R. J. Luebbers, F. Hunsberger and K. S. Kunz, "A Frequency-dependent Finite Difference Time-Domain Formulation for Transient Propagation in Plasma," IEEE Trans. Antennas and Propagat., vol. 39, pp. 29-34, 1991

[15] R. M. Joseph, S. C. Hagness and A. Taflove, "Direct Time Integration of Maxwell's Equations in Linear Dispersive Media with Absorption for Scattering and Propagation of Femtosecond Electromagnetic Pulses," Opt. Lett., vol. 16, pp. 1412-1414, 1991

[16] R. J. Luebbers and F. Hunsberger, "FDTD for Nth-order Dispersive Media," IEEE Trans. Antenna and Propagat., vol. 40, pp. 1297-1301, 1992

[17] F. Hunsberger, R. Luebbers and K. Kunz, "Finite-Difference Time-Domain Analysis of Gyrotropic Media-I: Magnetic Plasma," IEEE Trans. Antennas and Propagat., vol. 40, pp. 1489-1495, 1992

[18] R. Luebbers, D. Steich and K. Kunz, "FDTD Calculation of Scattering from Frequency-dependent Materials," IEEE Trans. Antennas and Propagat., pp. 1249-1257, 1993

[19] J. L. Young, "Propagation in Linear Dispersive Media: Finite Difference Time-Domain Methodologies," IEEE Trans. Antennas and Propagat., vol. 43, pp. 411-430, 1995

[20] Z. P. Liao, H. L. Wong, B. P. Yang and Y. F. Yuan, "A Transmitting Boundary for Transient Wave Analysis," Scientia Sinica, vol. XXVII, pp. 1063-1076, 1984

[21] A. Taflove, *Computational Electromagnetics: The Finite-Difference Time-Domain Method*, Boston: Artech House, 1995, pp. 42-44

[22] C. V. Hile and W. L. Kath, "Numerical Solution of Maxwell's Equations for Nonlinear-optical pulse propagation", Jour. of Soc. Am. B, vol. 13, No. 6, pp. 1135-1145, 1996

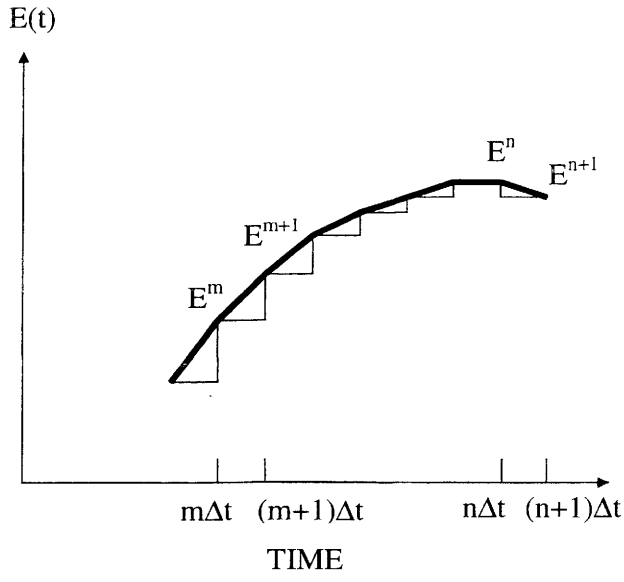

Figure 1: Illustration of the piecewise linear approximation for the electric field as a function of discrete time steps

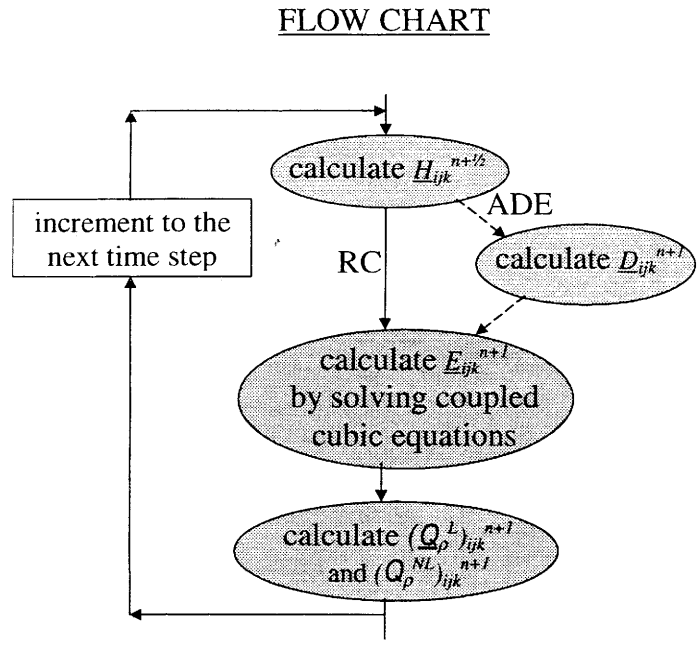

Figure 2: Flow chart to calculate electromagnetic field quantities for the recursive convolution (RC) approach and the auxiliary differential equation (ADE) approach

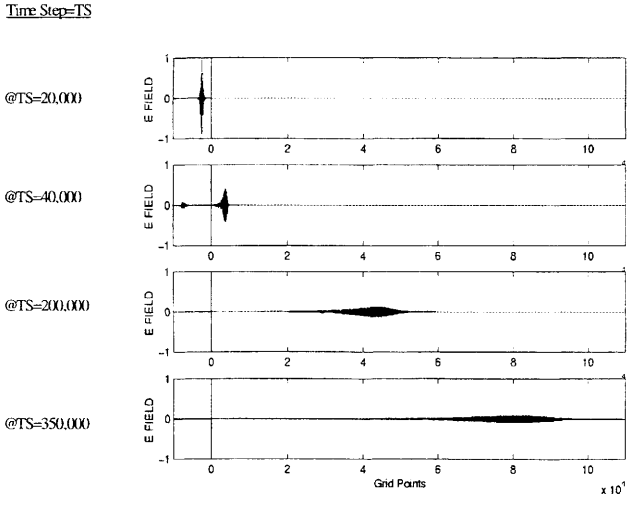

Figure 3: Time evolution of spatial electric field profiles inside the strictly linear dispersive medium

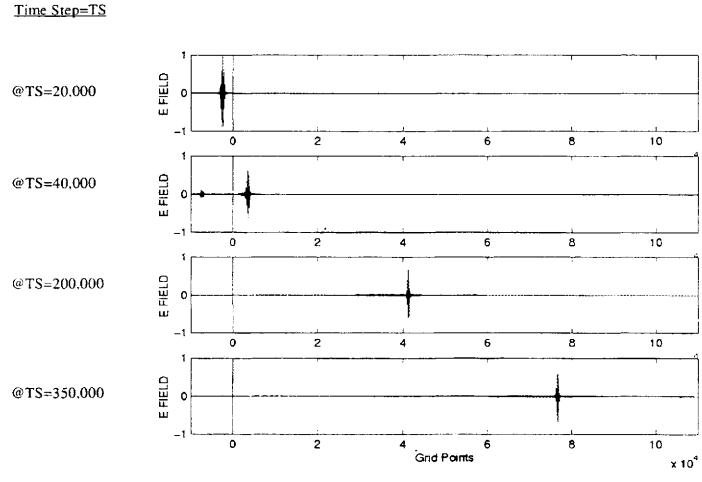

Figure 4: Time evolution of spatial electric field profiles inside the purely Kerr-type instantaneous nonlinear dispersive medium

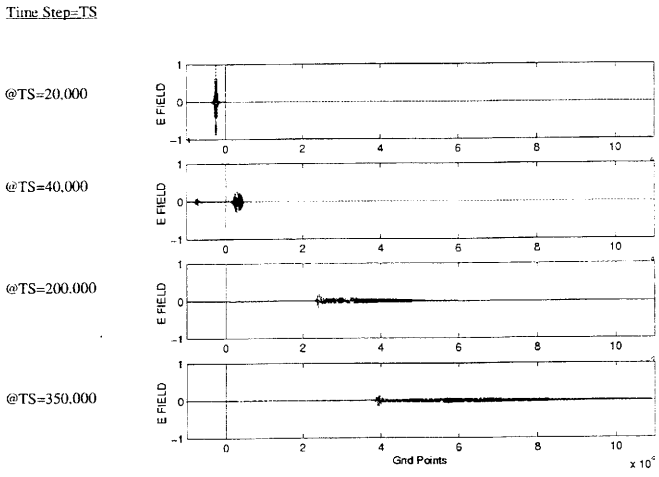

Figure 5: Time evolution of spatial electric field profiles inside the purely Raman scattering nonlinear dispersive medium

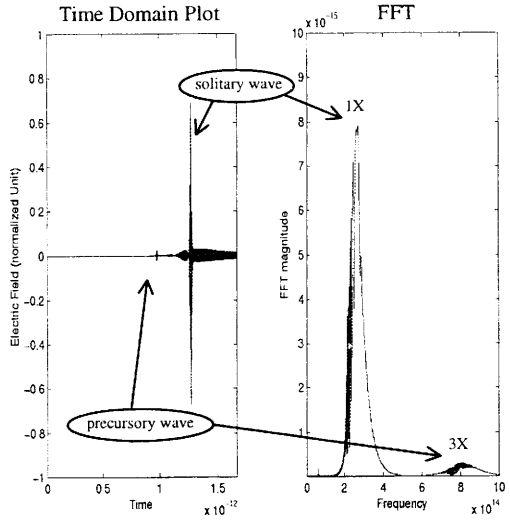

Figure 6: Time and FFT plots coming from the purely Kerr-type instantaneous nonlinear dispersive response at spatial location x = 40,000

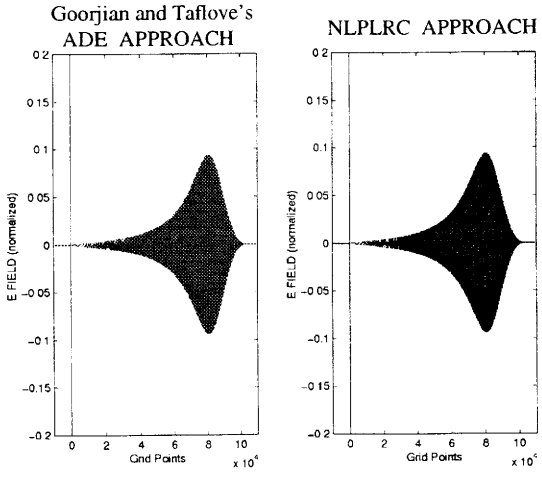

Figure 7: Comparison of our piecewise continuous recursive convolution approach to Goorjian and Taflove's auxiliary differential equation approach for the strictly linear dispersive case

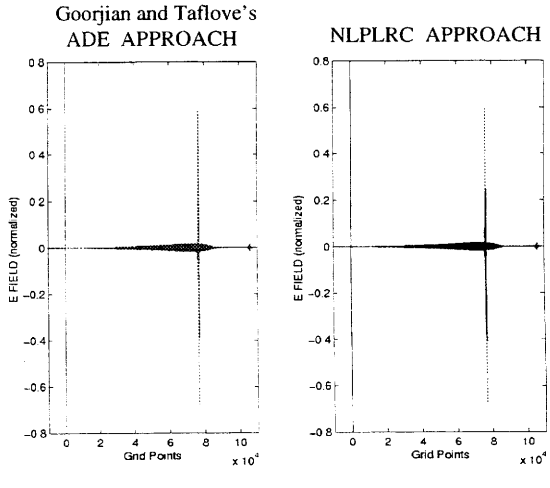

Figure 8: Comparison of our piecewise continuous recursive convolution approach to Goorjian and Taflove's auxiliary differential equation approach for the purely Kerr-type instantaneous nonlinear dispersive case

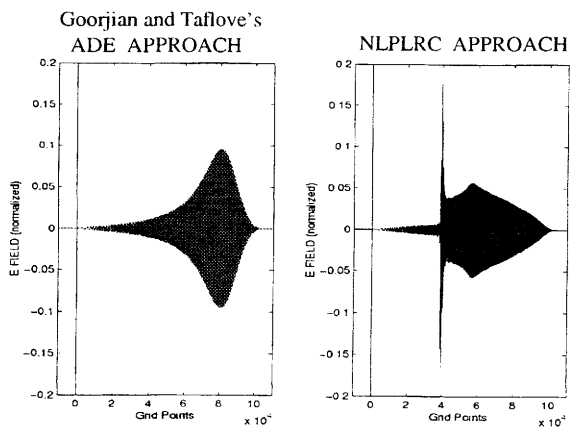

Figure 9: Comparison of our piecewise continuous recursive convolution approach to Goorjian and Taflove's auxiliary differential equation approach for the purely Raman scattering nonlinear dispersive case

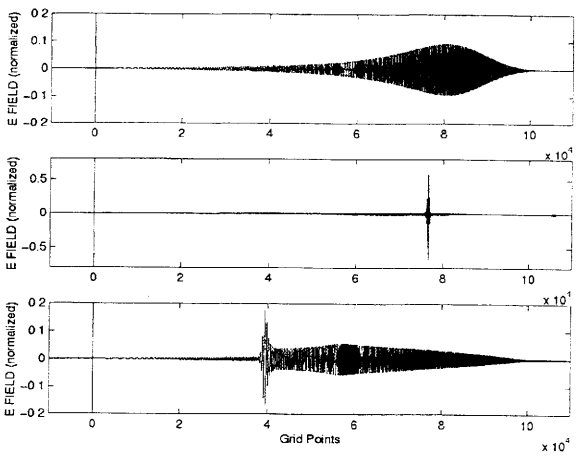

Figure 10: Relative comparison of spatial electric field profiles for a pulse propagating inside the strictly linear dispersive medium (top), the purely Kerr-type instantaneous nonlinear dispersive medium (middle) and the purely Raman scattering nonlinear dispersive medium (bottom) at time step=350,000

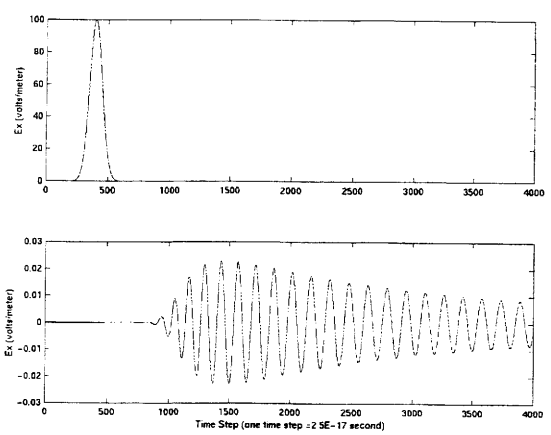

Figure 11: Temporal plots of a Gaussian driving pulse used to excite an optical TE_{10} mode and the resulting optical TE_{10} mode that is incident on the free-space/dispersive-material interface at the middle of the interface plane

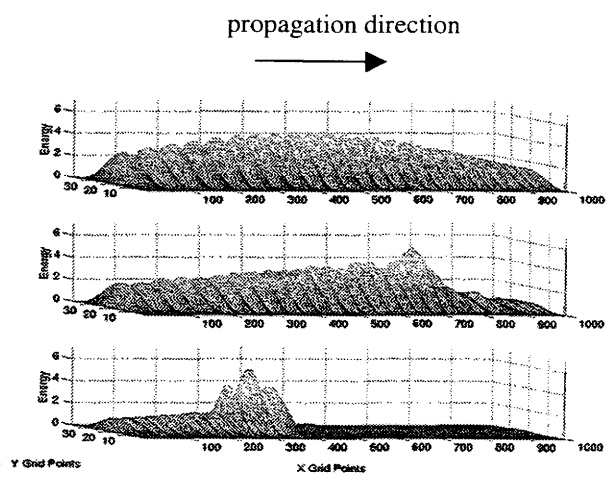

Figure 12: Comparison of spatial electromagnetic field energy density profiles from strictly linear dispersive (top), purely Kerr-type instantaneous nonlinear dispersive (middle) and purely Raman scattering nonlinear dispersive (bottom) cases at time step=7,500